

# B stars as a diagnostic of star-formation at low and high redshift

Duília F. de Mello

*Space Telescope Science Institute<sup>1</sup>, 3700 San Martin Drive, Baltimore, MD 21218*  
*e-mail: demello@stsci.edu*

Claus Leitherer

*Space Telescope Science Institute, 3700 San Martin Drive, Baltimore, MD 21218*  
*e-mail: leitherer@stsci.edu*

and

Timothy M. Heckman

*Physics and Astronomy Department, Johns Hopkins University, Homewood Campus, Baltimore, MD 21218*  
*e-mail: heckman@pha.jhu.edu*

## ABSTRACT

We have extended the evolutionary synthesis models by Leitherer et al. (1999b) by including a new library of B stars generated from the IUE high-dispersion spectra archive. We present the library and show how the stellar spectral properties vary according to luminosity classes and spectral types. We have generated synthetic UV spectra for prototypical young stellar populations varying the IMF and the star formation law. Clear signs of age effects are seen in all models. The contribution of B stars in the UV line spectrum is clearly detected, in particular for greater ages when O stars have evolved. With the addition of the new library we are able to investigate the fraction of stellar and interstellar contributions and the variation in the spectral shapes of intense lines. We have used our models to date the spectrum of the local super star cluster NGC 1705–1. Photospheric lines of C III  $\lambda$ 1247, Si III  $\lambda$ 1417, and S V  $\lambda$ 1502 were used as diagnostics to date the burst of NGC 1705–1 at 10 Myr. Interstellar lines are clearly seen in the NGC 1705–1 spectrum. Broadening and blueshifts of several resonance lines are stronger in the galaxy spectrum than in our models and are confirmed to be intrinsic of the galaxy. Si II  $\lambda$ 1261 and Al II  $\lambda$ 1671 were found to be pure interstellar lines with an average blueshift of 78 km s<sup>–1</sup> due to a directed outflow of the interstellar medium. We have selected the star-forming galaxy 1512–cB58 as a first application of the new models to high- $z$  galaxies. This galaxy is at  $z = 2.723$ , it is gravitationally lensed, and its high signal-to-noise Keck spectrum show features typical of local starburst galaxies, such as NGC 1705–1. Models with continuous star formation were found to be more adequate for 1512–cB58 since there are spectral features typical of a composite stellar population

---

<sup>1</sup>Operated by AURA for NASA under contract NAS5-26555

of O and B stars. A model with  $Z = 0.4 Z_{\odot}$  and an IMF with  $\alpha = 2.8$  reproduces the stellar features of the 1512-cB58 spectrum.

*Subject headings:* galaxies: evolution — galaxies: fundamental parameters — galaxies: starburst — galaxies: stellar content

*ApJ in press - February 10, 2000 - vol. 530*

## 1. Introduction

O and B stars with zero-age-main-sequence (ZAMS) masses  $\geq 5 M_{\odot}$  are the natural tracers of recent or current star-forming activity. These stars play a fundamental role in the evolution of a galaxy since they are responsible for the release of ionizing radiation, chemically enriched material, and kinetic energy via winds and supernovae (Maeder & Conti 1994). The most prominent stellar emission and absorption lines in the spectra of O and B stars are in the ultraviolet (UV) region. An old underlying stellar population and strong nebular emission lines may mask the contribution of a hot stellar population in the optical. Therefore, the preferred wavelength region to detect massive stars is longward of the Lyman  $\alpha$  forest but short enough to minimize spectral contamination from older stellar populations; i.e.  $1216 \text{ \AA} \leq \lambda \leq 2500 \text{ \AA}$ . Although this spectral region cannot be observed from the ground, the amount of high quality data obtained with the *International Ultraviolet Explorer* (IUE) has led to detailed spectral analyses of massive stars in the UV. The IUE spectral atlases of massive stars of Walborn, Nichols-Bohlin, & Panek (1985), Rountree & Sonneborn (1993) and Walborn, Parker, & Nichols (1995b) provide a unique tool for the spectral classification of O and B stars. Moreover, the IUE spectra have been extensively used to test stellar atmosphere models (e.g., Groenewegen & Lamers 1989).

Starbursts are a major mode of high-mass star formation. In the local universe four bright starburst galaxies (M 82, NGC 253, NGC 4945 and M 83) account for about 25% of the high-mass star formation rate (Heckman 1997). IUE, together with the Hubble Space Telescope (HST), and the Hopkins Ultraviolet Telescope (HUT) satellites, has dramatically increased our understanding of the starburst phenomenon (e.g., Huchra et al. 1983; Fanelli, O’Connell, & Thuan et al. 1988; Kinney et al. 1993; Leitherer et al. 1995a, 1996). The UV region of the starburst spectra is dominated by strong resonance transitions of, e.g., Si IV  $\lambda 1400$  and C IV  $\lambda 1550$ , which are the strongest spectral features of massive stars in the satellite-UV. The main contributors to the UV flux are O and early B stars. O stars dominate during the earliest starburst phase, when the spectra are characterized by broad ( $\sim 2000 \text{ km s}^{-1}$ ), highly ionized ( $\sim 50 \text{ eV}$ ) stellar wind lines. However, after a few million years O stars disappear, and B stars be-

come the main source of the UV flux in the integrated spectrum. Therefore, in order to analyze the stellar content of star-forming galaxies it is necessary to understand the contribution not only of O but also of B stars to the integrated spectra of these objects.

Evolutionary synthesis models were used by us before to analyze the integrated light of galaxies and to understand the hot-star content of local starburst galaxies (Robert, Leitherer, & Heckman 1993; Leitherer et al. 1996; Heckman & Leitherer 1997). We used Galactic O- and Wolf-Rayet stars as building blocks to synthesize the ultraviolet spectra of starburst galaxies in the local universe. A stellar library from IUE high-dispersion spectra was created and implemented into a synthesis code to model the ultraviolet spectra of O-star dominated starburst galaxies. The limitation of the synthesis technique is due to the uncertainties of the stellar evolution models and the quality of the stellar libraries used. Recently, in Leitherer et al. (1999b, hereafter Starburst99) we presented an upgrade of the models of Leitherer & Heckman (1995b). Starburst99 includes the newest model atmosphere grid of Lejeune, Cuisinier, & Buser (1997) and the latest Geneva evolutionary tracks. In this paper we present a new addition to Starburst99: a library of IUE high-dispersion spectra of B stars. With the addition of this new library we are able to synthesize high-resolution ( $0.75 \text{ \AA}$ ) UV spectra that are typical of more evolved starbursts ( $t > 10 \text{ Myr}$ ) dominated by B stars. We can also detect the contribution of B stars in young mixed populations which have high-ionization lines formed in O star winds but also have low-ionization lines from B supergiants. Section II describes the computational method. Section III introduces the new library of B stars and identifies the main diagnostic lines. Models for stellar population with different star formation laws and initial mass functions (IMF) are discussed in Section IV. Section V presents a set of synthetic models generated to reproduce the UV spectrum of the super star cluster in the local starburst NGC 1705, and Section VI discusses the stellar population of the high- $z$  galaxy 1512-cB58. Conclusions are presented in Section VII.

## 2. Method

Stars are generated in Starburst99 according to a star-formation law as a function of time and distributed along the ZAMS with a power-law IMF. The stars are evolved from the ZAMS using the evolu-

tionary models of the Geneva group. Two types of star-formation law are considered: (i) an instantaneous burst with no subsequent star formation and (ii) continuous star-formation at a constant rate. The stellar IMF is approximated by a power-law with an exponent  $\alpha$  and a lower and upper mass-limit  $M_{\text{low}}$  and  $M_{\text{up}}$ , respectively. The choices of IMFs are the Salpeter IMF with  $\alpha=2.35$ , and an approximate Miller-Scalo IMF with  $\alpha = 3.3$  (Salpeter 1955; Miller & Scalo 1979).  $M_{\text{low}}$  is assumed to be  $1 M_{\odot}$  and  $M_{\text{up}} = 100 M_{\odot}$ . A truncated Salpeter IMF with  $M_{\text{low}} = 1 M_{\odot}$  and  $M_{\text{up}} = 30 M_{\odot}$  is also available in Starburst99 but was not used in this work. We refer to Leitherer & Heckman (1995b) and Leitherer et al. (1999b) for more details on each individual parameter. Chemical evolution is not treated self-consistently in our models and each stellar generation has the same metallicity during the evolution of the population.

The proper transformation from the theoretical (effective temperature  $T_{\text{eff}}$ ; luminosity  $L$ ) to the observed (spectral type) plane is a concern in any evolutionary synthesis model. Recall that the theoretical prediction is  $T_{\text{eff}}$  and  $L$ , whereas the observed spectra are assigned via their corresponding spectral types. Therefore, the adopted  $T_{\text{eff}}$  vs. spectral type calibration becomes crucial. Starburst99 assigns spectral types to positions in the Hertzsprung-Russell diagram (HRD) using Schmidt-Kaler’s (1982) calibration. The choice of this calibration was validated by the success in reproducing both the integrated UV spectrum as well as the spectral type distribution of the ‘starburst Rosetta Stone’ 30 Doradus (Vacca et al. 1995). Schmidt-Kaler’s calibration has also been shown to agree with more recent calibration methods such as those of Chlebowski & Garmany (1991) for O-type stars and Humphreys & McElroy (1984) for later types (Massey et al. 1995).

B-supergiant dominated phases add a new challenge to the modeling: evolution proceeds very rapidly in those parts of the HRD where luminous B stars are located, and the star counts may be inaccurate if the interpolation scheme fails. Our scheme performs a nearest neighbor search in the  $L$  vs.  $T_{\text{eff}}$  plane to assign spectral types. We can test the reliability of our method by requiring that a constant star-formation model correctly reproduces the observed distribution of spectral types in the solar neighborhood within a few kpc from the Sun. If a sufficiently large volume is sampled, like for  $d \geq 1$  kpc, local variations of the

star-formation rate are expected to smooth out, and differences between theoretical and observed stellar statistics are primarily due to errors in the evolutionary model lifetimes, the spectral calibration, and the interpolation scheme. We performed this test by comparing the stellar population generated by our code with the observed number of massive stars compiled by Blaha & Humphreys (1989, BH hereafter). Their compilation includes luminous O and B stars and supergiants of all spectral types. Figure 1 of BH shows the HRD derived for stars in 91 associations and clusters within 3 kpc of the Sun. We used this figure to determine the number of stars for each spectral type. However, as shown by the luminosity function obtained by BH, the data are severely affected by incompleteness at  $M_V > -6$  (see Figure 8 in BH). Therefore, we have to take incompleteness into account before we compare the numbers predicted by our models with the numbers given in BH. We applied an incompleteness correction to the BH data in the following way. A first-order polynomial with slope = +0.71 was fitted to the luminosity function at  $-9 \leq M_V \leq -7$  where the data are still complete. The fit gives the expected number of stars for each  $M_V$ . The incompleteness factor for magnitude bins  $M_V > -7$  was determined by an extrapolation of the fitted line up to  $M_V \sim -4$  ( $M_V = -4.5$  for O9V stars). Applying this correction factor to BH’s data (using again Schmidt-Kaler’s calibration for the conversion from  $M_V$  to spectral type) we calculated the corrected number of stars for each spectral type. Table 1 shows the number of stars that were classified as OV and BI from BH’s data before and after correcting for incompleteness. Note the severe incompleteness of O main-sequence stars of all temperatures. In contrast, the visually brighter B supergiants of BH’s sample are almost complete. Table 1 also shows the predicted number of OV and BI stars generated by a model with Salpeter IMF, continuous star-formation law, and age = 20 Myr. The predicted spectral types become age-independent at this age since an equilibrium between star formation and stellar death has been reached. The observed and computed ratios OV/BI are 6.9 and 5.3, respectively. We did not attempt to optimize the agreement further, e.g. by varying the IMF, since the uncertainties due to the incompleteness correction by far exceed the 35% difference between the model and the observations. While the overall observed ratio of evolved over unevolved massive stars is reproduced rather well by our models, the detailed

supergiant distribution is not. The observed HRD shows a nearly flat distribution from early- to late-B supergiants, whereas the models predict an initial decrease and a subsequent increase for late B supergiants. This reflects the uncertainties of the details of the evolution models in these particular HRD regions. One should be aware that synthetic spectra showing mid- and late-B supergiant features are affected by this uncertainty. In practice, this should rarely be a concern. For an evolved single starburst population, the spectrum will be dominated by stars close to the main-sequence turn-off, and not by mid- to late-B supergiants. For a mixed population, mid- to late-B supergiants are present, but they hardly contribute to the spectrum due to their low UV flux. Nevertheless this caveat should be kept in mind. We conclude that our adopted  $T_{\text{eff}}$  vs. spectral type interface for B supergiants works reasonably well.

### 3. UV lines in O and B stars

O and B stars span a wide range of physical properties such as  $T_{\text{eff}}$ ,  $L$ , radius, and mass. O stars have  $T_{\text{eff}}$  in the range of  $3\text{--}5 \times 10^4$  K whereas B stars vary from  $1\text{--}3 \times 10^4$  K. Both are highly luminous with luminosities for O and B stars varying between  $2 \times 10^6\text{--}2 \times 10^5 L_{\odot}$  and  $1 \times 10^5\text{--}2 \times 10^2 L_{\odot}$ , respectively. Their luminosities are high enough to drive massive outflows in the form of radiation-driven stellar winds. The stellar radiation field below  $912 \text{ \AA}$  is the driving force of a wind (Lucy & Solomon 1970; Castor, Abbott, & Klein 1975). As the fraction of the stellar ionizing luminosity over the bolometric luminosity decreases from hot O stars to cooler B stars, the wind momentum decreases as well. Typical wind velocities for O stars are  $2\text{--}3 \times 10^3 \text{ km s}^{-1}$ , whereas for B stars the values are up to 10 times lower. At the same time, mass-loss rates decrease by at least an order of magnitude from spectral types O to B (e.g. Bieging, Abbott, & Churchwell 1989). Different wind properties and a softer ionizing radiation field dramatically modify the ultraviolet spectral morphology of B with respect to O stars: typical strong ultraviolet wind lines have lower ionization potentials in the 20 eV range (vs. 50 eV for O stars) and line widths and shifts of a few  $\text{\AA}$  (vs  $10 \text{ \AA}$  for O stars). Note that despite lower wind densities, B-star wind lines are still optically thick and therefore are strong features.

Typical UV spectra of O and B stars show three types of lines: stellar photospheric lines, stellar-wind

lines, and interstellar absorption lines. The most common ionized photospheric absorption lines are from C, N, O, Si, and Fe of low and high excitation potentials. Pure *photospheric lines* are formed in layers which are almost in hydrostatic equilibrium ( $v \lesssim 10^2 \text{ km s}^{-1}$ ) and are not affected by stellar wind outflows. Since these lines originate from excited levels, they do not form in stellar winds or in the interstellar medium (ISM). Therefore, they are a unique tracer of stars eliminating the uncertainty of contamination by an interstellar contribution. However, high-quality spectra are required for detection, as they are generally weak. The most notable exception is N IV  $\lambda 1720$  which forms in O-star winds despite originating from a highly excited level. It originates from the level  $^1P_0$  which is connected to the ground state  $^1S$  by an allowed line at  $\lambda 765 \text{ \AA}$ . This line is optically thick, so that the  $^1P_0$  state behaves as ground state. For very hot stars for which the Lyman continuum is less optically thick, the state will be depopulated by the photon escape from the resonance line at  $\lambda 765 \text{ \AA}$ . Strong resonance lines of any atomic and ionic species can form in *stellar winds* and in the *ISM*. Generally, species from lower ionization potentials are stronger in the ISM and lines from higher ionization potentials are stronger in winds. While this distinction is almost always true in O stars, it does not apply to B stars where it is often difficult to distinguish the stellar and interstellar components. Defining the contributions from the photosphere, wind, and ISM in B stars is one of the major goals of this paper.

Tables 2 and 3 summarize the main stellar and interstellar lines found in the spectra of O and B stars. The atomic data are from Moore (1950), except for C III  $\lambda 1426.45$ ,  $1427.84$  and S V  $\lambda 1501.76$  which were taken from van Hoof's line list at <http://www.pa.uky.edu/~peter/atomic>. The general trend in these tables is a decrease of the ionization potential of the dominant line with decreasing  $T_{\text{eff}}$  and with increasing contribution from the ISM. Tables 2 and 3 are intended to give the general trends in the spectral morphology of OB stars. Very often it is difficult to disentangle the stellar and interstellar components of a resonance line. An example is Si IV  $\lambda 1393.73$ ,  $1402.73$  (also called Si IV  $\lambda 1400$ ). This doublet has a strong wind contribution in giants and supergiants, and an additional weaker interstellar line. The stellar and interstellar components are usually easy to distinguish due to their large velocity separation. Si IV  $\lambda 1400$  is also a strong (unshifted) absorption line in OB main-

Table 1: Number of Stars for Each Spectral Type

Spectral Type	Number of Stars			Spectral Type	Number of Stars		
	Observed	Corrected	Predicted		Observed	Corrected	Predicted
O4V	2	3	201	B0I	27	43	633
O5V	8	26	411	B1I	32	51	668
O6V	30	120	1138	B2I	54	86	19
O7V	63	416	1730	B3I	28	45	15
O8V	99	792	3300	B5I	23	35	8
O9V	43	645	8880	B7I	2	2	4
				B8I	6	3	4
				B9I	8	13	518
Total	245	2002	15660		180	278	2974

sequence stars, reaching maximum strength around B1V. The lines become progressively weaker towards earlier and later types, with a corresponding increase in line strength of Si V and Si III transitions, respectively. The weak Si IV  $\lambda$ 1400 lines in the earliest O main-sequence stars are almost always interstellar, yet at IUE resolution their profiles are indistinguishable from those of photospheric lines. This degeneracy may be less of an issue when spectral morphology is concerned. It does, however, become crucial when Galactic stars are used as templates for comparison with starburst galaxies. The relative strengths of stellar and interstellar lines may well be different in those galaxies due to different ISM conditions. For this reason we attempted to describe the morphology of the stellar and interstellar lines separately in Tables 2 and 3.

Starburst99 includes a high-dispersion library of stellar types O and Wolf-Rayet and a low-dispersion library of B stars (see Robert et al. 1993 for a description of the libraries). This means that synthetic spectra generated to reproduce evolved bursts are composed mainly of low resolution ( $\sim 6 \text{ \AA}$ ) B star spectra which do not give enough detail for the line profiles. Therefore, in order to date an evolved burst and to study the stellar content of star-forming galaxies, a library of high-dispersion IUE spectra of B stars is needed. The inclusion of this library will also allow the study of the IMF in the intermediate-mass range. For example, a B8V star corresponds to a main-sequence mass of  $\sim 3 M_{\odot}$  with a lifetime of about 0.5 Gyr (Schaller et al. 1992) whereas O stars have ZAMS masses above  $\sim 20 M_{\odot}$  and lifetimes of less than 20 Myr.

We have used the atlases of IUE high-dispersion

spectra by Rountree & Sonneborn (1993) and Walborn et al. (1995b), and the sample by Howarth et al. (1997) as guidelines to select a library of B stars. Although these atlases are available in electronic version, these authors have only published rectified spectra. In order to be consistent with our previously generated library we have performed an independent extraction from the IUE archive and applied the same rules to the B-star library as we did in the case of O and WR stars. We have extracted high-dispersion, SWP, spectra from the IUE archive for all stars that showed no peculiarities in their spectra and that had IUE data from those atlases. The standard IUE processed data were considered to give reasonable results and no further calibration processing was needed. IDL was used to combine the echelle orders and the task *scombine* in IRAF to sum all the spectra of the same star. The number of spectra used in each star depended on the number of spectra available in the archive and their quality. For example, 10 spectra of HD 58350 (exposure times from 40 s to 120 s) were extracted from the IUE archive. After inspecting each spectrum, they were considered to show no peculiarity and all of them were used in the final summing. HD 79186, however, had only three spectra in the archive (exposure times 1200 s, 2520 s, and 3300 s) but they were considered of quality similar to HD 58350 and were used in the final summing.

Each spectrum was continuum normalized by dividing the calibrated spectra by a spline fit to the continuum. The task *continuum* in IRAF was used to perform the fit. This continuum normalization technique reveals prominent features such as a depression around 1400  $\text{\AA}$  and 1600  $\text{\AA}$ . As pointed out in Robert et al. (1999), these depressions are actually real features and are caused by Fe II, Fe III, Fe IV and Fe V

Table 2: Main OB Stellar Features

Ion	$\lambda$ (Å)	E.P. (eV) <sub>low</sub>	I.P. (eV) <sub>low</sub>	Comments
N V	1238.80	0.00	77.47	O3V–O6V, O3III–O9III, O3I–O9I B0III, B0I, B1I - wind see N V $\lambda$ 1238.80
C III	1242.78	0.00	77.47	O3V–O9V, O3III–O9III, O3I–O9I; stronger in $\geq$ O7
	1247.37	12.64	24.38	B0V–B8V, B0III–B8III, B0I–B8I; stronger in $\leq$ B2
S II	1250.50	0.00	10.36	IS in O stars; B0I–B8I stronger in $\geq$ B5
	1253.79	0.00	10.36	see S II $\lambda$ 1250.50
	1259.53	0.00	10.36	close to Si II $\lambda$ 1260.66
Si II	1260.66	0.00	8.15	purely IS in O stars
	1265.04	0.04	8.15	B0V–B8V, B0III–B8III, B0I–B8I - blended with IS
Si III	1294.55	6.51	16.34	B1V–B8V, B1III–B8III, B1I–B8I; stronger in $\geq$ B3
				O stars show Fe II in this region
				B0V–B8V, B0III–B5III, B0I–B8I
	1296.72	6.50	16.34	B0V–B8V, B0III–B3III, B0I–B8I - stronger in BIs
	1298.90	6.55	16.34	B0V–B8V, B0III–B8III, B0I–B8I - stronger in $\geq$ B2
Si II	1304.41	0.00	8.15	B3V–B8V, B3III–B8III, B3I–B8I - blended with IS, wind
	1309.28	0.04	8.15	B3V–B8V, B3III–B8III, B5I–B8I - blended with IS, wind
C II	1334.52	0.00	11.26	blended with C II $\lambda$ 1335.68 - IS
	1335.68	0.01	11.26	IS in O stars; B0V–B8V, blended with IS in $\geq$ B3V
				B0III–B8III, blended with IS in $\geq$ B5III
				B0I two components (IS C II $\lambda$ 1334.52)
				B1I–B8I blended with IS and show wind
Si IV	1393.73	0.00	33.49	O3V–O9V, O3III–O5III, O3I - no wind
				O6III–O9III wind, O4I–O9I - strong wind
				B0V–B8V stronger $\leq$ B3V, B0III–B3III wind in B0III
				B0I–B8I stronger $\leq$ B3I - strong wind
Si III	1402.73	0.00	33.49	see Si IV $\lambda$ 1393.73
	1417.20	10.23	16.34	O stars show Fe II lines in this region
				B2V–B8V, B6III–B8III, B0I–B8I stronger in $\leq$ B2I

Table 2: Main OB Stellar Features - Cont.

Ion	$\lambda$ (Å)	E.P. (eV) <sub>low</sub>	I.P. (eV) <sub>low</sub>	Comments
C III	1426.45	29.53	24.38	close to Fe V $\lambda$ 1429,1430 in O stars
				B0V, B1V, B0I–B2I, B0III–B2III
	1427.84	29.53	24.38	see C III $\lambda$ 1426.45
Si II	1485.40	6.83	8.15	close to N IV] in O stars
				B3V–B8V, B3III–B8III, B5I–B8I - weaker in BIs
S V	1501.76	15.76	47.30	O3V–O9V, O3III narrow, O5III–O9III, O3I–O9I
Si II				B0V, B1V, B0I, B1I
	1526.70	0.00	8.15	O5III–O9III, two blended components
				B0V–B8V, B0III–B8III, B0I–B8I, two blended components
	1533.44	0.04	8.15	O stars show Fe IV in this region
				B0V–B3V two components, B4V–B8V only IS
				B0III–B3III two components, B5III–B8III only IS
				B0I–B8I two blended components
C IV	1548.19	0.00	47.89	O3V–O7V, O3I–O5I - strong wind
				O3III–O9III, O6I–O9I
	1550.77	0.00	47.89	B0V, B0III, B0I–B3I - strong wind
Fe II	1608.45	0.00	7.87	O3V, O4V, O3III–O7III - two blended components
				$\geq$ O5V, O3I–O9I - only IS
				B0V–B8V, B0III–B8III, B1–B8I, two blended components
He II	1640.49	40.64	24.59	O3V–O9V, O3III–O9III; stronger in $\geq$ O7
				O3I–O5I - wind, O6I–O9I
				B0V, B1V, B0III, B1III, B0I–B3I
Al II	1670.81	0.00	5.99	IS in O stars
				B0V–B8V stronger $\geq$ B5V, B5III–B8III, B1I–B8I
N IV	1718.52	16.13	47.45	similar to Si IV $\lambda$ 1400 in O stars
				close to Al II/III blend in B stars

Table 3: Main Interstellar Features

Ion	$\lambda$ (Å)	E.P. (eV) <sub>low</sub>	I.P. (eV) <sub>low</sub>
N V	1238.80	0.00	77.47
	1242.78	0.00	77.47
S II	1250.50	0.00	10.36
	1253.79	0.00	10.36
	1259.53	0.00	10.36
Si II	1260.66	0.00	8.15
O I	1302.17	0.00	0.00
Si II	1304.41	0.00	8.15
C II	1334.52	0.00	11.26
	1335.68	0.01	11.26
Si IV	1393.73	0.00	33.49
	1402.73	0.00	33.49
Si II	1526.70	0.00	8.15
C IV	1548.19	0.00	47.89
	1550.77	0.00	47.89
Fe II	1608.45	0.00	7.87
Al II	1670.81	0.00	5.99

lines. These Fe ions are diagnostics of massive stars. Very few of them are transitions from the ground state which make them unlikely to be formed in the interstellar medium.

The final library was built with 73 B stars of spectral types B0–B8 and luminosity classes I, III, V (Table 4). We generated average spectra for each spectral type and luminosity class. For example, the class B0.5I spectrum is made by averaging the spectra of HD 38771, HD 150898, HD 152234, HD 167756, and HD 185859. Figure 1 illustrates the differences between individual stars and the average spectrum. Overall the average spectrum preserves the main features common in each individual spectrum. Features which are not strong in all stars are smoothed out in the average spectrum. Therefore, one should take into account that using average spectra may create uncertainties in the final generated spectrum. However, the average spectra suit the qualitative application of our method. Classes II and IV were not taken from the IUE archive. They were created by taking the average between the nearest luminosity classes; i.e.  $IV = (III + V)/2$  and  $II = (I + III)/2$ .

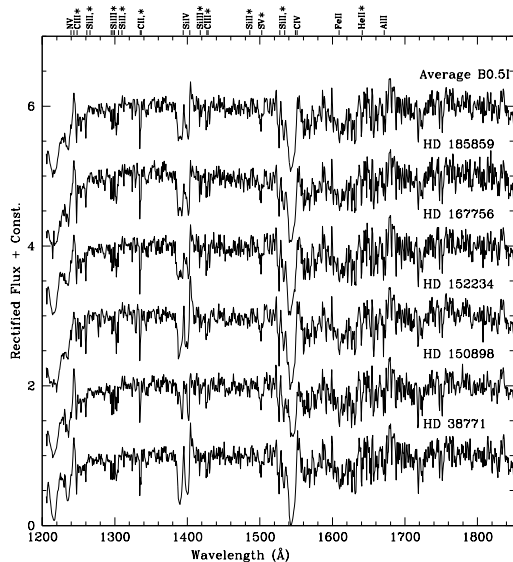


Fig. 1.— Rectified spectra of B0.5I stars and the average spectrum. Star names are given on the right corner of each spectrum. Excited lines (photospheric) are marked with “\*”. “,\*” is used when only the second component is an excited line. See Table 4 for a list of stars. The spectra are rectified.

Figure 2 shows representative spectra of our library. It is important to notice that most of the features seen in the IUE stellar spectra are real physical lines and not noise (Nemry, Surdej, & Hernaiz 1991). Several features are important diagnostics in B stars. Silicon, for example, has been shown to be a good diagnostic for the evolutionary state of a star because the atmospheric abundance is expected to remain unchanged by nuclear processing (e.g. Walborn 1971; Prinja 1990). In the following we will discuss those diagnostics in more detail which have the greatest potential in constraining extragalactic populations.

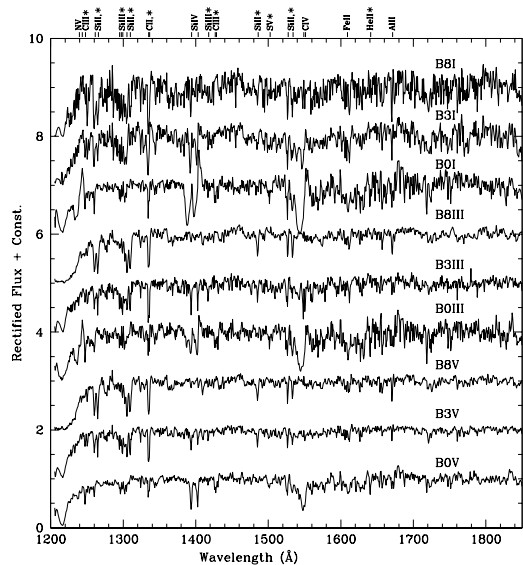


Fig. 2.— Rectified spectra of representative B stars. Spectral types are given on the right corner of each spectrum. Spectral types with more than one spectrum were averaged. Excited lines (photospheric) are marked with “\*”. “,\*” is used when only the second component is an excited line. See Table 4 for a list of stars. The spectra are rectified.

### 3.1. Silicon lines

Si II  $\lambda 1260.66$ ,  $1265.04$  are found in B stars of all luminosity classes. Si II  $\lambda 1260.66$  is a strong interstellar line in O and B stars (Figure 3). Si II  $\lambda 1265.04$  is photospheric and is not seen in O stars. The irregular shape of Si II  $\lambda 1265.04$  suggests the presence of Si II  $\lambda 1264.73$  but with the spectral resolution ( $0.75 \text{ \AA}$ ) of our library we cannot separate the two lines.



Table 4: B Stars - IUE Library

Spectral Type	Stars	Spectral Type	Stars	Spectral Type	Stars
B0V	HD 53755 HD 143275 HD 149438	B0III	HD 48434	B0I	HD 37128 HD 91968 HD 122879
B0.5V	HD 55857 HD 144217	B0.5III	HD 218376 HD 332407	B0.5I	HD 38771 HD 150898 HD 152234 HD 167756 HD 185859
B1V	HD 31726 HD 37018 HD 144470	B1III	HD 23180 HD 147165	B1I	HD 106343 HD 148422 HD 148688 HD 150168 HD 163522 HD 190603
B1.5V	HD 35299 HD 36959				
B2V	HD 42401 HD 64802	B2III	HD 35468	B2I	HD 41117 HD 42087 HD 92964 HD 116084
B2.5V	HD 148605 HD 175191				
B3V	HD 32630 HD 74280 HD 120315 HD 190993	B3III	HD 79447	B3I	HD 53138 HD 75149 HD 111973 HD 225093
B4V	HD 20809 HD 65904				
B5V	HD 25340 HD 34759 HD 188665	B5III	HD 22928 HD 34503	B5I	HD 58350 HD 79186 HD 1000943
B6V	HD 90994	B6III	HD 23302		
B7V	HD 17081 HD 29335 HD 87901				
B8V	HD 23324	B8III	HD 23850	B8I	HD 34085

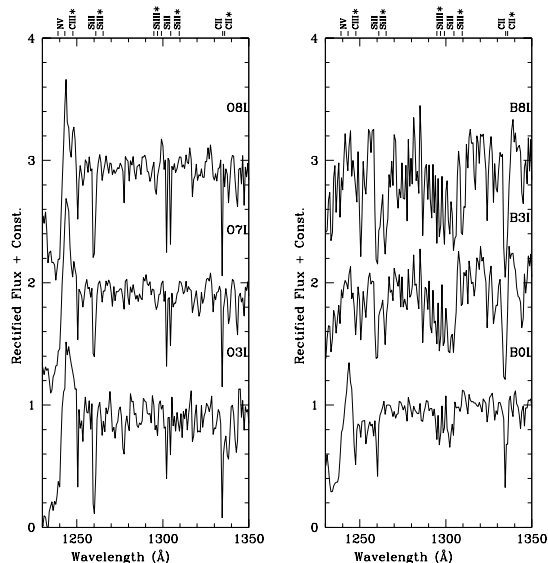


Fig. 3.— Spectral region around 1300 Å in O (left) and B (right) supergiants. The strongest features are labeled. Excited lines (photospheric) are marked with “\*”.

The Si III  $\lambda 1295$ – $1300$  photospheric lines are formed by six lines in the multiplet  $^3P^0$ – $^3P$ . Three lines, Si III  $\lambda 1294.55$ ,  $\lambda 1296.72$ , and  $\lambda 1298.90$  are found in B stars of all luminosity classes. Si III increases in strength through late B supergiants and it is absent in O supergiants (Figure 3). The blending with O I  $\lambda 1302.17$  (pure interstellar line), Si II  $\lambda 1304.41$ , and Si II  $\lambda 1309.28$  enhances the Si III strength in late type stars if the 1300 Å region is observed at low spectral resolution.

The Si IV  $\lambda 1393.73$ ,  $1402.73$  resonance line doublet develops from photospheric plus interstellar in the luminosity class V spectrum, through intermediate wind profiles at class III, to a full P Cygni profile in the luminosity class I. This is due to the fact that there is a correlation between luminosity and wind density. Only luminous stars have stellar winds dense enough to generate enough opacity to produce a strong P Cygni profile. Figure 4 shows the behavior of these lines for early B stars. The change in the Si IV  $\lambda 1400$  profile with luminosity class makes it a powerful diagnostic of B stars. These lines are essentially absent in stars later than B5.

The Si III  $\lambda 1417.20$  photospheric line is seen in stars of spectral classes B2V–B8V, B6III–B8III and

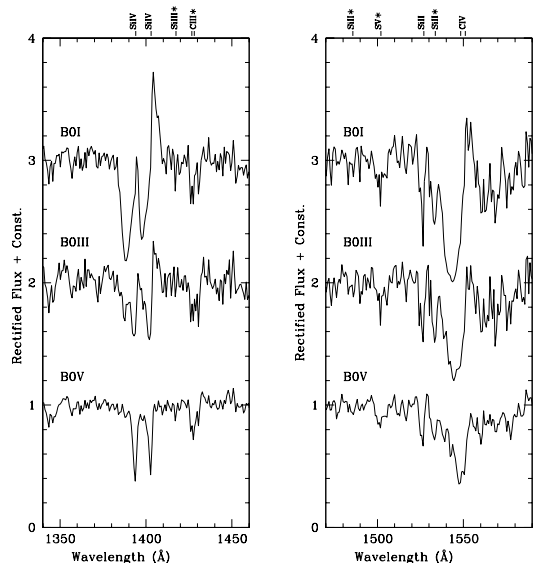


Fig. 4.— Spectral region around 1400 Å (left) and 1525 Å (right) in B0 stars. Excited lines (photospheric) are marked with “\*”.

in all supergiants. The maximum strength of this line is in early B supergiants.

Si II  $\lambda 1485.40$  is seen in stars of spectral classes B3V–B8V, B3III–B8III, and B5I–B8I. It is stronger in later BVs and BIII. This line originates from an excited level. Consequently it is purely stellar without interstellar contamination and can be used as a unique tracer of mid- to late-B stars.

Si II  $\lambda 1526.70$ ,  $1533.44$  are located in a region contaminated by the P Cygni profile of C IV  $\lambda 1548.19$ ,  $1550.77$ . The resonance line of Si II  $\lambda 1526.70$  has a narrow and deep interstellar component whereas Si II  $\lambda 1533.44$  is photospheric. Figure 4 shows the change of these lines in early B stars as a function of luminosity class. The maximum strength of Si II  $\lambda 1533.44$  is reached in early B supergiants. O stars have Fe IV lines in this region.

### 3.2. Carbon and sulfur lines

C III  $\lambda 1247.37$  and C III  $\lambda 1426.45$ ,  $1427.84$  are purely photospheric lines. C III  $\lambda 1247.37$  is seen in O and B stars of all luminosity classes. It is stronger in stars later than O7. In B stars it becomes stronger in stars earlier than B2. It can be blended with Fe IV  $\lambda 1246.8$ ,  $1247.8$  and be affected by the N V  $\lambda 1240$  P Cygni profile. C III  $\lambda 1426.45$ ,

1427.84 are seen only in early B stars. They are close to Fe V  $\lambda$ 1429, 1430 in O stars.

C II  $\lambda$ 1334.52, 1335.68 are interstellar and photospheric lines, respectively. Due to its small excitation potential of 0.01 eV, the  $\lambda$ 1335.68 line can sometimes be observed as an interstellar line as well. Only the interstellar line is seen in O stars due to the low ionization potential of C II. B stars, however, show either the two components (B0I and B0III to B3III) or a broad line formed by the two lines blended (B3V to B8V, B5III to B8III and B1I to B8I). BIs show P Cygni profiles (right panel in Figure 3 and Figure 5, which will be discussed later in the next section).

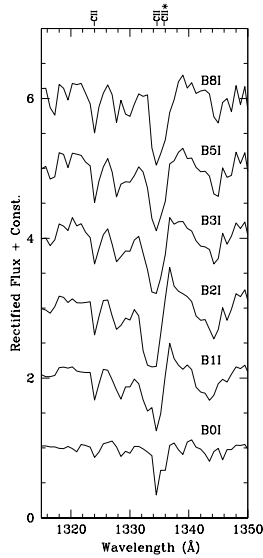


Fig. 5.— Spectra of B supergiants showing C II  $\lambda$ 1335, 1336 (see Table 4 for a list of stars). Excited lines (photospheric) are marked with “\*”. The spectra are rectified.

C IV  $\lambda$ 1548.19, 1550.77 (also called C IV  $\lambda$ 1550) are the strongest stellar lines in O stars in the satellite-UV. O3V to O7V and O3I to O5I show strong P Cygni profiles that dominate the spectral region. In B stars these lines are strong only in B0V, B0III and B0I–B3I. The changes of the profiles for different luminosity classes are shown in Figure 4. C IV  $\lambda$ 1548.19, 1550.77 are essentially absent in types later than B5 when the ionization balance shifts towards C III and C II.

S V  $\lambda$ 1501.76 is seen in most O stars of all luminosity classes and spectral types. In B stars it is seen

only in early types. This line has no interstellar contribution since it originates from an excited level.

#### 4. Population models: varying the IMF and SF

We computed a series of models to explore the effects of varying the IMF and the star-formation (SF) law. In Figure 6 we show the results for the Salpeter IMF using an instantaneous SF for several ages (5–300 Myr). Several spectral features clearly vary with age and are powerful diagnostics for age-dating bursts of star formation. For instance, lines such as C III  $\lambda$ 1247, Si II  $\lambda$ 1261, 1265, Si II  $\lambda$ 1304, 1309, C II  $\lambda$ 1335, 1336, Si IV  $\lambda$ 1400, Si II  $\lambda$ 1485, Si II  $\lambda$ 1527, 1533, C IV  $\lambda$ 1550, and Al II  $\lambda$ 1671 are quite conspicuous and are age dependent. A few resonance lines are of interstellar origin as we discussed earlier (Table 3). One of the most striking spectral features is C IV  $\lambda$ 1550 which has the strongest P Cygni profile. This feature is typical of hot stars with rapidly flowing winds and becomes less pronounced with age. Si IV  $\lambda$ 1400 shows a similar behavior. However, due to larger optical depth of the C<sup>3+</sup> ion, C IV shows a P Cygni profile at earlier ages, confirming the results by Robert et al. (1993).

Another conspicuous feature is around  $\lambda$ 1300. As we discussed in the previous section, this wavelength region is very rich in absorption features due to Si III  $\lambda$ 1295, 1297, 1299, O I  $\lambda$ 1302, Si II  $\lambda$ 1304, 1309. The Si III photospheric lines become stronger at greater ages. Figure 7 shows how the line profiles vary with age in this region of the spectrum. Si II  $\lambda$ 1304, 1309 are a very good age indicator; both lines get stronger at greater ages. Although the  $\lambda$ 1304 line may have an interstellar contamination in star-burst spectra.

The variation of the Si II  $\lambda$ 1261, 1265 doublet with age (see Figures 6 and 7) is particularly useful to contrast stellar and interstellar lines. The two transitions originate from multiplet (4) of Si II (Moore 1950).  $\lambda$ 1261 is from the ground level whereas  $\lambda$ 1265 comes from an excited level. In the absence of interstellar contamination and if wind effects are negligible, the strength of both lines should vary with spectral type in a similar manner. Si II  $\lambda$ 1261 is also formed in B-star winds. Inspection of the atlas of Walborn et al. (1995b) indicates that Si II  $\lambda$ 1261 shows the same spectral-type dependence as Si II  $\lambda$ 1265, suggesting that  $T_{\text{eff}}$  is the prime driver for the behavior

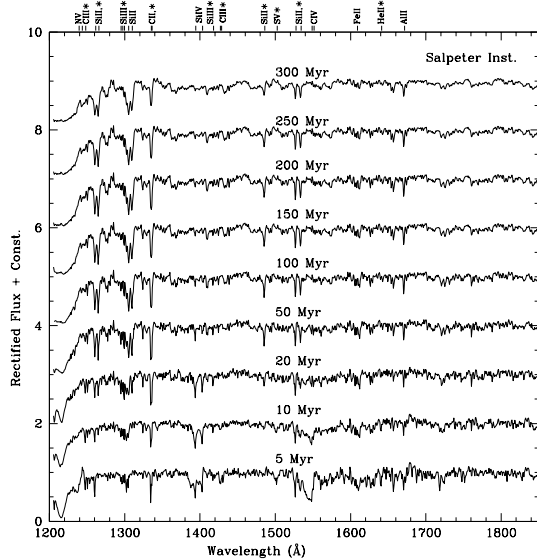


Fig. 6.— Synthetic spectra between 5 and 300 Myr. Star-formation law: instantaneous; IMF: Salpeter; solar metallicity. Excited lines (photospheric) are marked with “\*”. “,\*” is used when only the second component is an excited line. The spectra are rectified.

of both lines and that density effects are secondary. Therefore the time variation of Si II  $\lambda 1265$  in Figure 6 indicates the ‘true’ time variation of the stellar population. The Si II  $\lambda 1261$  component carries - in principle - the same information but the strong interstellar contribution to this line cannot be separated at the resolution of Figure 6. Recall that the stars used in the libraries are not free of interstellar lines; they are stars in the Milky Way and have interstellar lines in their spectra. Interstellar lines usually are blended or are very close to photospheric and wind lines which makes the identification and removal very difficult. In early O stars, for instance, it is not possible to distinguish between a weak photospheric and interstellar line around Si IV  $\lambda 1400$  (Leitherer, Robert, & Heckman 1995c). With the addition of the B library to our code we can investigate the relative proportion of the stellar and interstellar contribution to the resonance lines. From Figure 7 it is clear that predominantly interstellar lines such as Si II  $\lambda 1261$  show a very small variation with age in contrast with the photospheric line Si II  $\lambda 1265$ . The same is true for the interstellar line O I  $\lambda 1302$ .

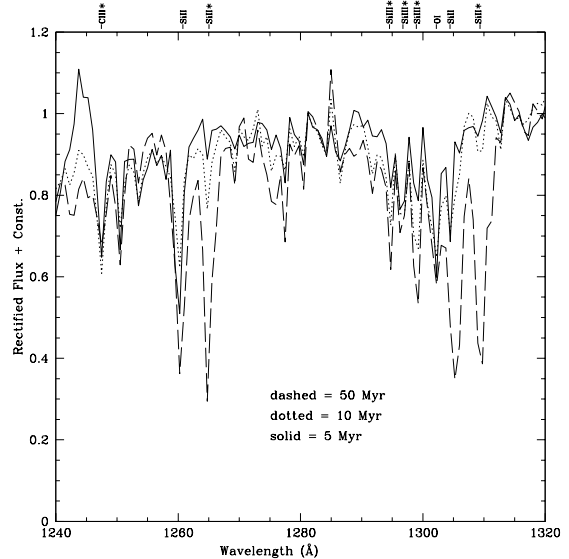


Fig. 7.— Synthetic spectra for the wavelength region 1240-1320 Å at 5 Myr (solid line), 10 Myr (dotted line) and 50 Myr (dashed line). Star-formation law: instantaneous; IMF: Salpeter; solar metallicity. Excited lines (photospheric) are marked with “\*”. The spectra are rectified.

The C II  $\lambda 1335$ ,  $\lambda 1336$  profile variation with age is shown in Figure 8. For small ages, when O stars are present, C II  $\lambda 1335$  is a deep and narrow interstellar line. However, for greater ages it shows as a broader profile. Since these spectra were generated by accessing our stellar libraries we searched for stars that have similar spectral shape. We found that stars of type B3V show the same broad photospheric C II line (right panel in Figure 8). Therefore, C II  $\lambda 1335$ ,  $\lambda 1336$  has a strong B-star contribution. As shown in Figure 5, this line has a noticeable P Cygni profile in B1 and B2 supergiants.

The age effect in the Si IV  $\lambda 1400$  and C IV  $\lambda 1550$  profiles is shown in Figure 9. The P Cygni profile typical of O stars dominates in early ages. It is absent in the 50 Myr model. The pollution of P Cygni profiles by photospheric iron lines has to be taken into account when analyzing these features (Nemry et al. 1991). For instance, when O stars are present (5 Myr model in Figure 9) we detect Fe V  $\lambda 1388$  and Fe IV  $\lambda 1533$  but after the burst has evolved we start detecting Si II  $\lambda 1533$  typical of B stars. C III  $\lambda 1426$ ,  $\lambda 1428$  also shows a strong dependence on age but there are

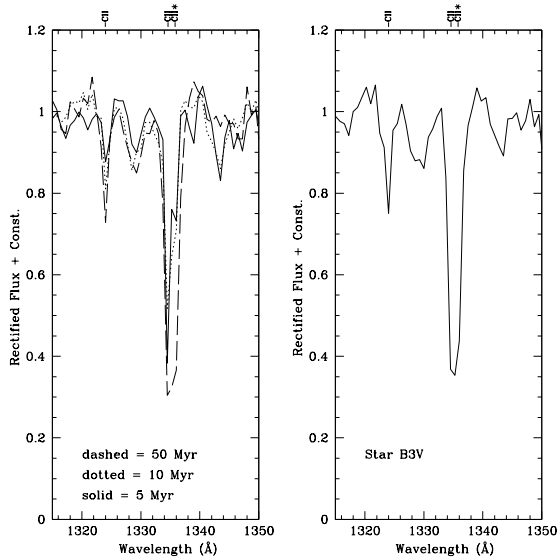


Fig. 8.— Left panel: Synthetic C II profiles around 1335 Å at 5 Myr (solid line), 10 Myr (dotted line) and 50 Myr (dashed line). Star-formation law: instantaneous; IMF: Salpeter; solar metallicity. Right panel: Same spectral region in a B3V star from our library (average of 4 stars - see Table 4 for a list of stars). Excited lines (photospheric) are marked with “\*”. The spectra are rectified.

several iron lines (Fe IV, V  $\lambda$ 1426-1429) in this region, and it is not possible to deblend their contribution accurately. Another feature that shows a strong age effect is Si II  $\lambda$ 1485 which appears after 20 Myr.

Since the IMF and the star-formation history play a fundamental role in defining the stellar population of a star-forming region, we have generated models also for a Miller-Scalo IMF, which is steeper than Salpeter and produces fewer massive stars. In Figure 10 we show the UV spectra for an instantaneous burst for ages 5 to 100 Myr. In comparison with a Salpeter IMF, a Miller-Scalo IMF produces more B and fewer O stars. Therefore the spectra in Figure 10 have correspondingly stronger B-star features at a given age than the spectra in Figure 6. Compare, for instance, the strength of the features at  $\lambda$ 1300 and  $\lambda$ 1400 at 5 Myr. In Figures 11 and 12 we show models for continuous SF for Salpeter and Miller-Scalo IMFs. The variation in the spectral shapes of strong lines such as Si IV  $\lambda$ 1400 and C IV  $\lambda$ 1550 is a powerful diagnostic for the interpretation of the spectra

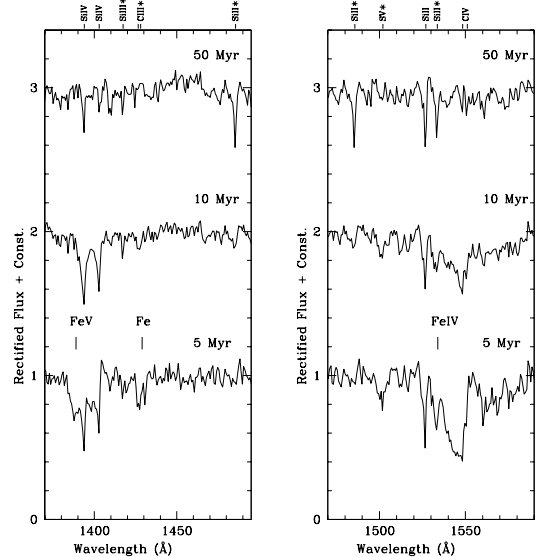


Fig. 9.— Synthetic spectra at 5 Myr, 10 Myr, and 50 Myr showing the spectral region around 1400 Å (left) and 1550 Å (right). The iron lines labeled as “Fe” are a blend of Fe IV-V ( $\lambda$ 1426-1429). Star-formation law: instantaneous; IMF: Salpeter; solar metallicity. Excited lines (photospheric) are marked with “\*”. The spectra are rectified.

of starburst galaxies. However, an age-IMF degeneracy is present and should be taken into account. For example, note the similarity between the model with a Salpeter IMF, continuous SF and age 100 Myr and the model with a Miller-Scalo IMF, continuous SF and age 10 Myr. This is due to the fact that both models generate the same number of massive stars producing the UV light. While it is often difficult to disentangle age and IMF effects with UV spectra only, the *duration* of the star formation can be constrained to some extent. Consider the Salpeter IMF models for instantaneous (Figure 6) and continuous (Figure 11) star formation. The presence of low-ionization lines from B stars and high-ionization lines from O stars is anticorrelated for instantaneous burst models. The B-star features at  $\lambda$ 1265,  $\lambda$ 1309, or  $\lambda$ 1335 are only strong when the O-star features at  $\lambda$ 1400,  $\lambda$ 1501, or  $\lambda$ 1550 have disappeared, and vice versa. This is no longer true in the mixed population of Figures 11 and 12. Both low- and high-ionization stellar lines are conspicuous, indicating O and B stars. This provides a strong constraint on the starburst duration.

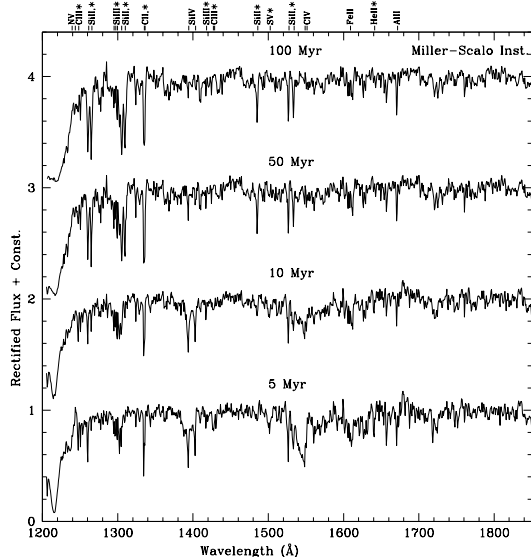


Fig. 10.— Synthetic spectra between 5 and 100 Myr. Star-formation law: instantaneous; IMF: Miller-Scalo; solar metallicity. The spectra are rectified. Excited lines (photospheric) are marked with “\*”. “,\*” is used when only the second component is an excited line.

## 5. Modeling NGC 1705 - a local starburst

NGC 1705 is a blue compact dwarf at a distance of 6.2 Mpc (Meurer et al. 1995). A super star cluster, NGC 1705-1, probably created during a burst  $10^7$  years ago, has a core diameter of 2 pc and is responsible for 50% of the total UV emission of NGC 1705 (Melnick, Moles, & Terlevich 1985; Meurer et al. 1992; Meurer et al. 1995). Because NGC 1705-1 is both exceptionally bright and of high surface brightness in the UV, it has one of the highest signal-to-noise UV starburst spectra taken with the HST Goddard High Resolution Spectrograph (GHRS). This galaxy was extensively discussed by York et al. (1990), Heckman & Leitherer (1997) and Sahu & Blades (1997), and we refer to those papers for further information on the kinematics of its interstellar medium. An age of about 10 Myr for the burst has been estimated based on the strength and shape of the line profiles. Thus, the NGC 1705-1 UV line spectrum is dominated by the light from B stars. Furthermore, the small size of NGC 1705-1 favors small starburst durations, which makes it highly likely that a single (instantaneous) population is ob-

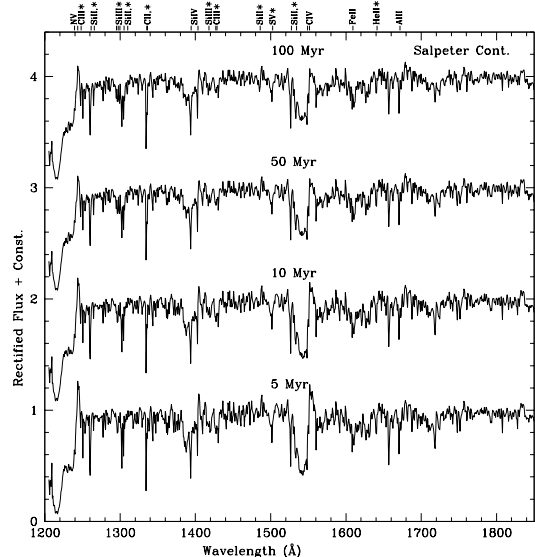


Fig. 11.— Synthetic spectra between 5 and 100 Myr. Star-formation law: continuous; IMF: Salpeter; solar metallicity. Excited lines (photospheric) are marked with “\*”. “,\*” is used when only the second component is an excited line. The spectra are rectified.

served. Therefore this cluster is a perfect case to test our method; i.e. we can assess how accurately the new B stellar library is able to model the UV spectra of local star-forming galaxies.

NGC 1705 has an oxygen abundance of  $\sim 0.45 Z_{\odot}$  (Marlowe et al. 1995), whereas the stars in our library have solar, or somewhat subsolar metallicity. However, the opacity effects in the photospheric features of hot stars are significant only at metallicities lower than the LMC (Lejeune et al. 1997). Therefore, for NGC 1705-1 it is adequate to use the solar metallicity tracks in the models together with the stellar library. In Figure 13 we show the spectrum of NGC 1705-1 together with models for instantaneous bursts of 5, 10, and 20 Myr for a Salpeter IMF and solar metallicity. We have binned the spectrum of NGC 1705-1 in order to have the same resolution as the stellar library (0.75 Å).

Many of the spectral features that are not well reproduced in our models are actually identified as interstellar lines of NGC 1705-1 and/or of the Milky Way halo (see Heckman & Leitherer 1997 for a detailed identification of these features). Figure 14 shows the 10 Myr model and the spectrum of NGC 1705-

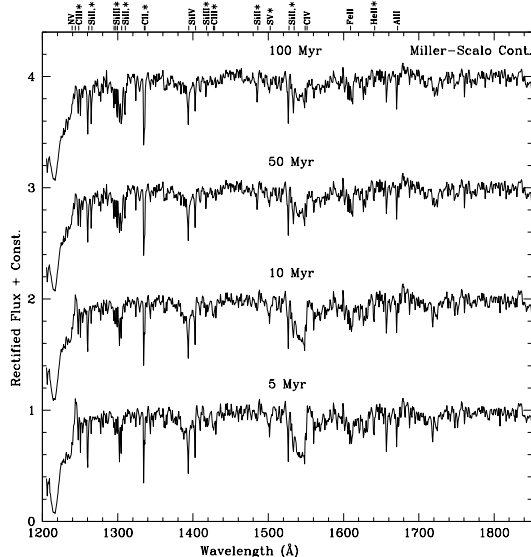


Fig. 12.— Synthetic spectra between 5 and 100 Myr. Star-formation law: continuous; IMF: Miller-Scalo; solar metallicity. Excited lines (photospheric) are marked with “\*”. “,\*” is used when only the second component is an excited line. The spectra are rectified.

1. Interstellar lines are deep and narrow and much stronger in the star cluster than in our models. This is due to the fact that starburst galaxies have larger interstellar velocity dispersions and therefore their spectra present stronger interstellar lines than the library stars. An initial comparison between our models and NGC 1705–1 indicates that an age of 5 Myr old is probably too small, showing too strong wind lines typical of O stars (N V, Si IV and C IV). The 20 Myr old model is probably too old, showing features typical of late type B stars (e.g. Si II  $\lambda$ 1485) and lacking features of late O and early type B stars (e.g. S V  $\lambda$ 1502) present in the star cluster spectrum. The best way to date the burst is to avoid interstellar lines and utilize pure stellar lines. The stellar lines C III  $\lambda$ 1247, Si II  $\lambda$ 1265, Si III  $\lambda$ 1295, 1297, 1299, Si III  $\lambda$ 1417, C III  $\lambda$ 1426, 1428, Si II  $\lambda$ 1485, S V  $\lambda$ 1502, and Si II  $\lambda$ 1533 are pure photospheric lines. However, some of them are in regions very close to strong interstellar lines and should be used with caution. We chose C III  $\lambda$ 1247, Si III  $\lambda$ 1417, and S V  $\lambda$ 1502 as age diagnostics. We have applied a  $\chi^2$  test to all ages of the models for each of these lines. A significantly lower  $\chi^2$  is found at 10 Myr suggest-

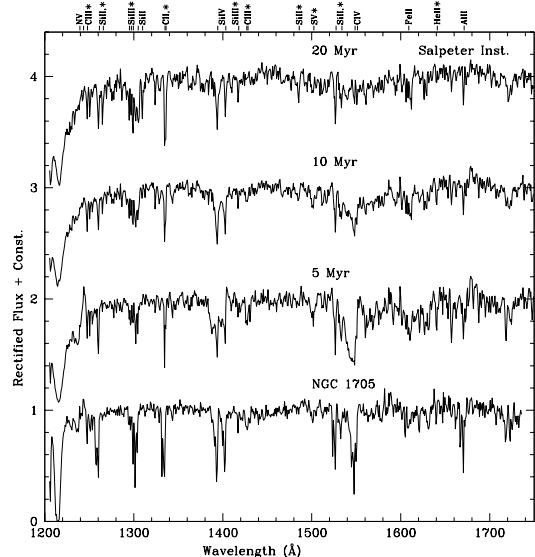


Fig. 13.— Spectrum of NGC 1705–1 and synthetic spectra for ages 5, 10, and 20 Myr. Salpeter IMF, instantaneous star-formation and solar metallicity. Excited lines (photospheric) are marked with “\*”. “,\*” is used when only the second component is an excited line. The spectra are rectified.

ing that the 10 Myr old burst model is the one that best reproduces the spectral features of the star cluster, in agreement with Heckman & Leitherer (1997). We have inspected our models in order to verify the spectral type of B stars which are contributing to the synthetic spectra. At 10 Myr there are no more O stars (the last generation of O stars is seen at 7 Myr), and most of the B-star population is composed of BVs and early BII stars. Therefore, the photospheric lines such as C III  $\lambda$ 1247, Si III  $\lambda$ 1417, and S V  $\lambda$ 1502 seen in the 10 Myr model originate in these stars.

Inspection of the observed NGC 1705–1 spectrum shows broadening and blueshifts of the resonance lines. Their origin was discussed by Heckman & Leitherer (1997). The unblended resonance lines Si II  $\lambda$ 1527 and Al II  $\lambda$ 1671 illustrated in Figure 15 were used in their analysis. Heckman & Leitherer concluded that these two lines were interstellar and that large-scale inhomogeneities and macroscopic motions in the interstellar medium were the main mechanism generating the shape and shifts. With the addition of the B star library we can address the stellar contribution in more detail. Figure 15 shows 5 Myr,

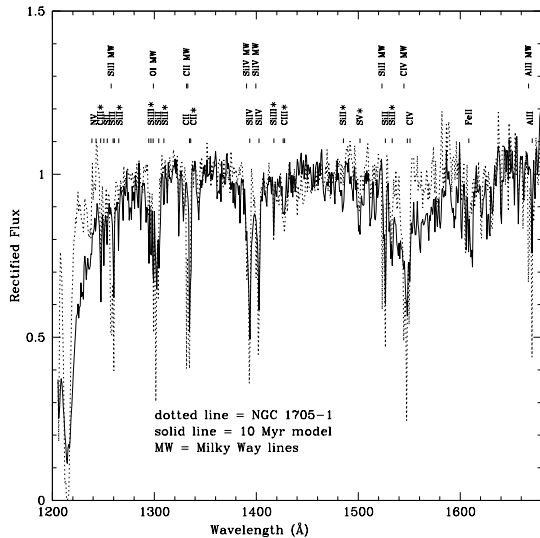


Fig. 14.— Spectrum of NGC 1705-1 (dotted line) and synthetic spectrum at 10 Myr (solid line). Salpeter IMF, instantaneous star-formation. Milky Way lines are identified as “MW”. Excited lines (photospheric) are marked with “\*”. The spectra are rectified.

10 Myr and 50 Myr models for the Si II  $\lambda 1527$  and the Al II  $\lambda 1671$  regions. Photospheric lines of Si II  $\lambda 1485$  and S V  $\lambda 1502$  and wind lines of C IV  $\lambda 1550$  clearly show an age effect while Si II  $\lambda 1527$  and Al II  $\lambda 1671$  show no significant variation with age. This behavior suggests that Si II  $\lambda 1527$  and Al II  $\lambda 1671$  are interstellar. For comparison, we have marked the interstellar line C I  $\lambda 1657$  (Walborn et al. 1985) in Figure 15 which shows a similar behavior to Si II  $\lambda 1527$  and Al II  $\lambda 1671$ .

A more quantitative way of identifying interstellar (IS) lines requires measurements of their full width at half-maximum (FWHM). Pure IS lines should have the same FWHM independent of age and any time dependent broadening would be due to a stellar component. The FWHM of Al II  $\lambda 1671$  in our models remains of the order of  $\sim 1.2$  Å from 8 to 40 Myr. After that the stellar component starts dominating the profile and the FWHM reaches  $\sim 1.7$  Å at 60 Myr. Therefore, since Al II  $\lambda 1671$  is pure interstellar at 10 Myr, we confirm the interstellar nature of Al II  $\lambda 1671$  in NGC 1705-1. Si II  $\lambda 1261$  shows a similar behavior and it is also interstellar at 10 Myr. Other lines such as C II  $\lambda 1335$ , Si II  $\lambda 1527$ , Si IV  $\lambda 1400$ ,

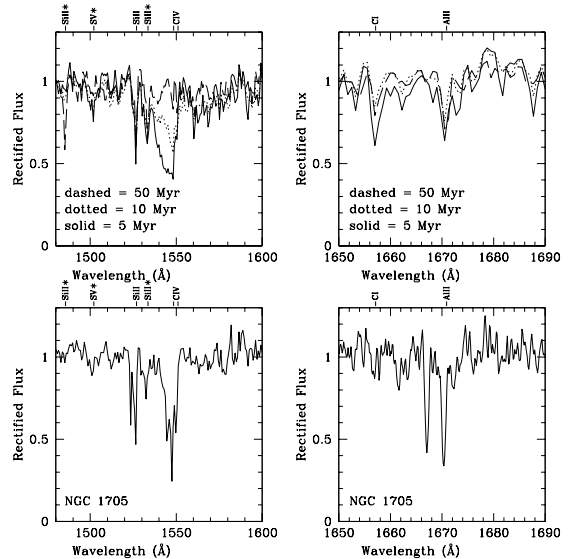


Fig. 15.— Lower panels: Spectrum of NGC 1705-1 showing the spectral regions around  $\lambda 1550$  Å and  $\lambda 1670$  Å. Upper panels: Synthetic spectra at ages 5 (solid line), 10 (dotted line), and 50 (dashed line) Myr. Salpeter IMF, instantaneous star-formation and solar metallicity. Excited lines (photospheric) are marked with “\*”. The spectra are rectified.

and C IV  $\lambda 1551$  have blended components and/or extended blue wings which affect the measurements of the FWHM. We estimate that Si IV  $\lambda 1400$  has about equal contributions from B-star photospheric and from interstellar lines. In order to measure the blueshifts of these IS lines in NGC 1705-1, we have generated a residual spectrum by subtracting the 10 Myr model from the spectrum of NGC 1705-1. The residual spectrum shown in Figure 16 contains IS lines of NGC 1705-1 and Galactic lines. The blueshift determination requires accurate measurements of the central wavelengths of each line. However, most of the residual lines have complex profiles, except for the pure IS lines of Si II  $\lambda 1261$  and Al II  $\lambda 1671$ . They are blueshifted by  $56 \text{ km s}^{-1}$  and  $100 \text{ km s}^{-1}$ , respectively. Therefore, we conclude that an average blueshift of  $78 \text{ km s}^{-1}$  is due to a directed outflow of the IS medium in NGC 1705-1.

## 6. Modeling high- $z$ galaxies

We have selected the star-forming galaxy 1512-cB58 as a first application of our models to galaxies



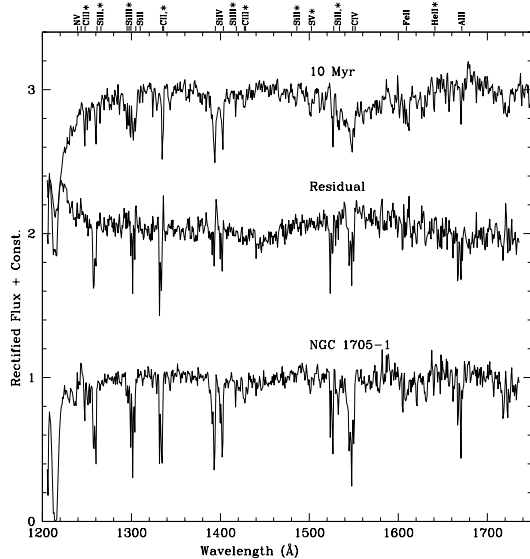


Fig. 16.— Spectrum of NGC 1705-1, synthetic spectrum at 10 Myr, and residual spectrum (10 Myr model subtracted from NGC 1705-1). Excited lines (photospheric) are marked with “\*”. “,\*” is used when only the second component is an excited line. The spectra are rectified.

whose stellar content is still largely unknown. 1512-cB58 is at  $z = 2.723$  and was serendipitously discovered by Yee et al. (1996) during the observation of the cluster MS1512+36 at  $z = 0.373$  (Gioia & Luppino 1994) with the 3.6m Canada-France-Hawaii Telescope as part of the CNOC project (The Canadian Network for Observational Cosmology). Ellingson et al. (1996) estimated that 1512-cB58 is a factor of 20 brighter in the  $V$  band than galaxies in the sample of Steidel et al. (1996). Seitz et al. (1998) using HST images have modeled the gravitational lens and showed that 1512-cB58 is lensed into a gravitational fold arc by the cluster. The part of the source of 1512-cB58 which is mapped into the arc is reconstructed by their models, and its magnification is found to be  $\mu_{\text{arc}} \geq 50$ . They suggest that this galaxy is not intrinsically bright but just a ‘normal’ star-forming galaxy at high- $z$ . Because of its flux magnification, observations with Keck can reach a signal-to-noise of 50, better than achievable for local starburst galaxies, in just 11,400 s. We used the spectrum shown in Pettini et al. (1999), which has a resolution of  $3.5 \text{ \AA}$  ( $= 0.94 \text{ \AA}$  in the restframe), in our analysis. The spectrum was continuum normalized by dividing the spectrum by a spline fit to the

continuum, following the same procedure as applied to the stars in the library. We confirm the identification of the absorption lines by Yee et al. (1996) and used the IRAF task *dopcor* to correct for the redshift. Figure 17 shows the spectrum of 1512-cB58 together with the spectrum of NGC 1705-1 plotted in rest wavelengths. The absorption lines around  $1370 \text{ \AA}$  in the spectrum of 1512-cB58 are identified as Mg II  $\lambda 2796, 2803$  at  $z = 0.82$ . Some telluric sky residuals are seen at  $1500 \text{ \AA}$ .

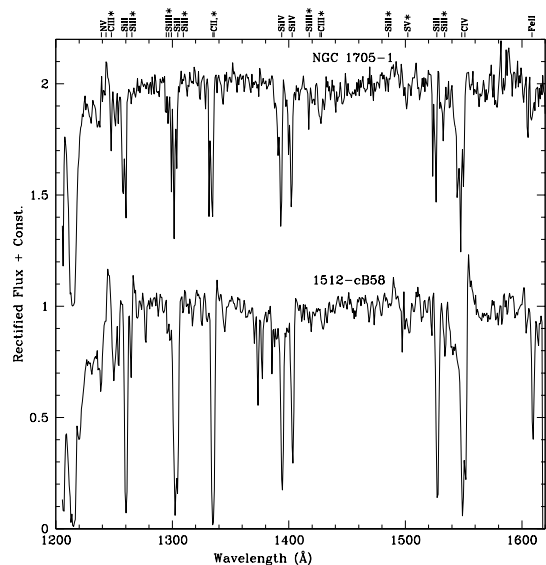


Fig. 17.— Keck spectrum of 1512-cB58 (Pettini et al. 1997) and GHRs spectrum of NGC 1705-1 (Heckman & Leitherer 1997). Excited lines (photospheric) are marked with “\*”. “,\*” is used when only the second component is an excited line. The spectra are rectified and plotted in the restframe wavelength system.

The limitations of our method and the quality of the spectrum should be taken into account before choosing the models that are suitable for 1512-cB58. Two main issues should be considered. (i) Our method works better for objects closer to solar metallicity since the library is composed of stars from the solar vicinity. Therefore, for galaxies at high- $z$ , which are expected to have lower metallicity (Pettini 1999), we can only change the metallicity of the tracks in the models while using the available stellar library. Later in this section, we will show that this change is able to produce spectral features similar to the ones found in 1512-cB58. (ii) The biggest concern in this method

is the contamination of diagnostic lines by interstellar lines. Interstellar lines are the strongest lines in the spectrum of 1512-cB58 and, even more than in NGC 1705-1, they contaminate all B-star wind lines. The strength of the interstellar lines is due to a large interstellar velocity dispersion caused by large-scale inhomogeneities and macroscopic motions in the interstellar medium.

Nevertheless, there are several features that can be used to analyze the stellar content of 1512-cB58. Two of the most remarkable features in the spectrum of 1512-cB58 are the P Cygni profiles of N V  $\lambda$ 1240 and C IV  $\lambda$ 1550. Dey et al. (1997) have identified P Cygni profiles in another high- $z$  galaxy, the radio galaxy 4C 41.17 at  $z = 3.8$ . They concluded that the P Cygni profiles are formed in stellar winds of massive stars in 4C 41.17. It is unlikely that a galactic outflow is the origin of the P Cygni profiles due to the large outflow mass required to produce them. The same reasoning can be used to infer that the P Cygni profiles in 1512-cB58 are *stellar*, as opposed to *interstellar*. Therefore, the presence of N V  $\lambda$ 1240 and C IV  $\lambda$ 1550 indicates the existence of O stars in 1512-cB58.

Figure 18 shows the spectral region where photospheric and wind lines are seen in the spectrum of 1512-cB58. Two models for a Salpeter IMF and instantaneous SF at 4 Myr and 15 Myr, and one model for a Salpeter IMF and continuous SF at 50 Myr are also shown in Figure 18. In the left panel the identification of B stars in the spectrum of 1512-cB58 is confirmed by the presence of the low-ionization photospheric lines of Si II  $\lambda$ 1265 and Si III  $\lambda$ 1295-1300. In the spectrum of 1512-cB58 these lines are more similar to the 15 Myr model, which is dominated by B stars, than to the 4 Myr model which is dominated by O stars. The spectral resolution of 1512-cB58's spectrum ( $0.94 \text{ \AA}$ ) is sufficient to resolve Si II  $\lambda$ 1265 from the interstellar Si II  $\lambda$ 1261. However, even though the resolution should be enough to separate the Si III  $\lambda$ 1295-1300 lines, they are blended together with the intrinsically very broad Si II  $\lambda$ 1304 resonance line. In the right panel the presence of B stars is confirmed by the strong photospheric line of Si II  $\lambda$ 1533. Thus, we conclude that the continuous SF model shows lines typical of O *and* B stars and is therefore a better match to the spectrum of 1512-cB58.

We conclude that there is evidence for a composite stellar population of both O and B stars in the

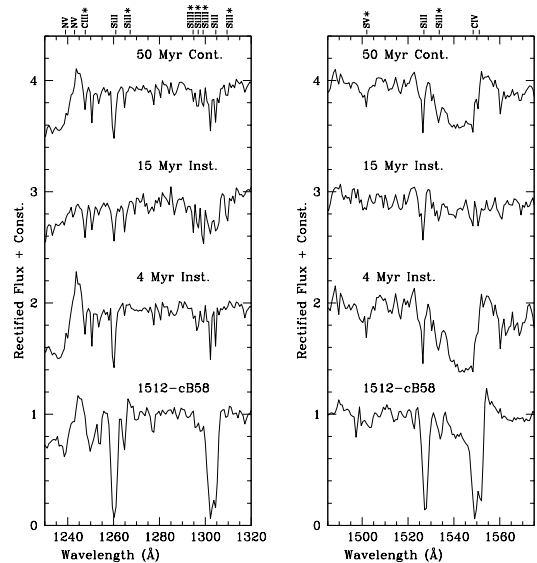


Fig. 18.— Spectral regions around  $\lambda$ 1280  $\text{\AA}$  and  $\lambda$ 1530  $\text{\AA}$  of 1512-cB58. Synthetic spectrum for Salpeter IMF, instantaneous star-formation at 4 and 15 Myr, and continuous star-formation at 50 Myr; solar metallicity. Excited lines (photospheric) are marked with “\*”. The spectra are rectified.

spectrum of 1512-cB58. In this case, the starburst in 1512-cB58 is extended in time. This is consistent with the fact that it is also spatially-extended: the entire object was placed inside the aperture, due to the small apparent size of the galaxy. This is very different from the super star cluster, NGC 1705-1. The integrated spectrum of NGC 1705-1 comes from a single point source whereas in 1512-cB58 the integrated light comes from the whole galaxy. In the spectrum of NGC 1705-1 there are no signatures of O stars, like the P Cygni profiles of N V  $\lambda$ 1240 and C IV  $\lambda$ 1550. On the other hand, there are many features typical of B stars as we discussed in Section V.

We have generated models for 1512-cB58 taking into account that spatially-extended starbursts are represented better by a continuous SF than by an instantaneous burst. Figure 19 shows three synthetic spectra, together with the spectrum of 1512-cB58. The first model was generated with a Salpeter IMF for continuous SF and solar metallicity. The second model was generated with a Miller-Scalo IMF for continuous SF and solar metallicity. Both models are at 100 Myr. The precise age has little effect

on the computed spectrum in continuous SF models if  $t \geq 20$  Myr. Most of the features shown in both models are also seen in the spectrum of 1512-cB58. As in NGC 1705-1 the interstellar lines are stronger in the galaxy than in our models due to macroscopic motions in the ISM of both objects. Another major difference between the models and the spectrum of 1512-cB58 is the fact that the wind lines are too strong in the Salpeter IMF model and too weak in the Miller-Scalo IMF model with solar metallicity. Taking into account that high- $z$  galaxies may have SMC- to LMC-like metallicity (Pettini 1999) and that properties of the absorption lines in local starbursts depend strongly on metallicity and IMF (Heckman et al. 1998; Leitherer 1999a; Robert et al. 1999), we have generated a third model changing these parameters. We used an IMF slope  $\alpha = 2.8$  and sub-solar metallicity for the *tracks* ( $Z = 0.4Z_{\odot}$ ). Although the stellar library has solar metallicity, the change in the metallicity of the stellar tracks and the steeper IMF causes a significant change in the wind lines. They are not as strong as in the ones produced by the model with Salpeter IMF and solar metallicity. The P Cygni profile of N V  $\lambda 1240$  resembles better the one in 1512-cB58 than the previous models. However, the strength of the absorption component of C IV  $\lambda 1550$  is greater in 1512-cB58 than in the model. This is due to the fact that the interstellar line is much stronger in the galaxy than in the model. The deep absorption trough between 1545 and 1552 Å (Figure 18 right panel) is entirely interstellar. This becomes immediately obvious from an inspection of C IV  $\lambda 1550$  profiles in individual O stars (Walborn et al. 1985). Stellar winds never produce profiles which become black immediately shortward of the emission peak. Rather, they gradually reach the minimum intensity after several hundred  $\text{km s}^{-1}$ , level off, and approach the continuum level after about 2000  $\text{km s}^{-1}$ . This simply results from the opacity vs. velocity relation in O-star winds. Applied to the spectrum of 1512-cB58, the stellar part of the absorption component of C IV  $\lambda 1550$  is the ‘bulge’ seen at  $\sim 1540$  Å in Figure 18. It is this ‘bulge’ (and the emission component) relative to the Si II  $\lambda 1533$  which gives the relative number of O vs. B stars.

Pettini et al. (1999) and Ellingson et al. (1996) dated the burst of 1512-cB58 at 20 and 35 Myr, respectively. We generated models for those ages and compared with the 100 Myr model (Figure 20). As mentioned earlier, the precise age of the burst has

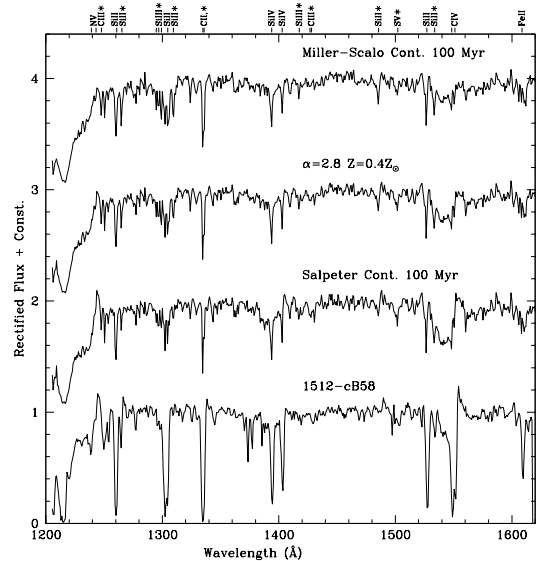


Fig. 19.— Spectrum of 1512-cB58 and synthetic spectra for three models: Salpeter IMF, continuous star-formation, 100 Myr, solar metallicity; Miller-Scalo IMF, continuous star-formation, 100 Myr, solar metallicity; IMF slope  $\alpha=2.8$ , continuous star-formation, 100 Myr, metallicity  $Z = 0.4 Z_{\odot}$ . Excited lines (photospheric) are marked with “\*”. “,” is used when only the second component is an excited line. The spectra are rectified.

little effect on the computed spectrum in continuous SF models for  $t > 20$  Myr. However, the absence of Si II  $\lambda 1485$  in the galaxy spectrum and its strength in the models suggest that the burst is probably younger than 100 Myr but older than 20 Myr.

We used the magnitudes measured by Ellingson et al. (1996) to calculate the star-formation rate (SFR) for 1512-cB58 that is implied by our models (see Table 5). We have first increased the fluxes by 3.6 magnitudes and 1.6 magnitudes at  $V$  and  $K$  respectively to correct for the effects of dust-extinction. These values are based on the  $UV$  colors of the galaxy, the precepts of Meurer, Heckman, & Calzetti (1999), and the empirical starburst dust attenuation law of Calzetti (1997). We have then corrected the fluxes downward by a factor of 50 to account for the estimated lensing magnification (Seitz et al. 1998). Luminosities ( $\lambda P_{\lambda}$ ) were computed taking  $H_0 = 50 \text{ km s}^{-1} \text{ Mpc}^{-1}$  and  $q_0 = 0.5$ . The resulting intrinsic bolometric luminosity for 1512-cB58 is  $\sim 1.5 \times 10^{12} L_{\odot}$ . The

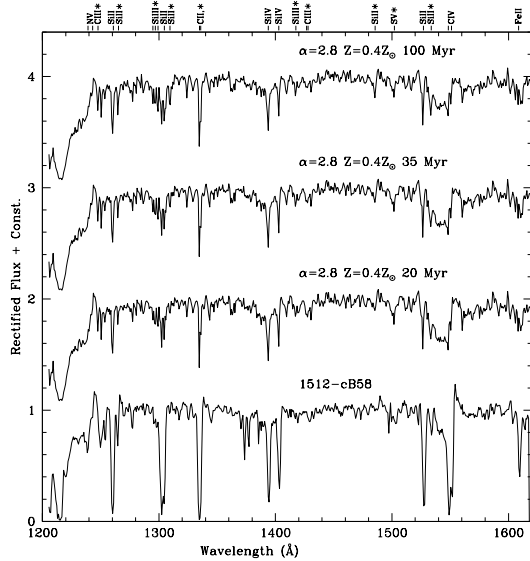


Fig. 20.— Spectrum of 1512-cB58 and synthetic spectra for three models: IMF slope  $\alpha=2.8$ , continuous star-formation, 20, 35, and 100 Myr, metallicity  $Z = 0.4 Z_{\odot}$ . Excited lines (photospheric) are marked with “\*”. “,\*” is used when only the second component is an excited line. The spectra are rectified.

SFR was then calculated by comparing these final luminosities with the predicted values from the Starburst99 models for a Salpeter IMF,  $1-100 M_{\odot}$ ,  $Z = 0.4 Z_{\odot}$ , and continuous star-formation for  $t = 100$  Myr. The resulting SFR for 1512-cB58 is estimated to be 83 and  $44 M_{\odot} \text{ yr}^{-1}$  based on the luminosities at rest-wavelengths of  $1480 \text{ \AA}$  and  $5750 \text{ \AA}$  respectively. Note that a conventional Salpeter IMF extending down to  $0.1 M_{\odot}$  would lead to SFR values that are 2.55 times larger. For such a normal IMF, the stellar mass formed over 100 Myr would be  $\sim 2 \times 10^{10} M_{\odot}$ , or about 20% of the stellar mass of a present-day Schechter  $L_*$  galaxy. We are evidently witnessing a major galaxy-building event in 1512-cB58. In any case, while the luminosity and implied SFR for 1512-cB58 are near the high-end of the estimated extinction-corrected values for UV-selected ‘U dropout’ galaxies at this redshift, they are not extraordinary (e.g. Meurer, Heckman, & Calzetti 1999).

We have also compared our models with another high- $z$  lensed galaxy, the Arc 384 in the Abell 2218 cluster (Ebbels et al. 1996), kindly provided by R. Ellis. The spectrum was continuum normalized and

corrected for redshift ( $z = 2.515$ ) following the same procedure as applied to 1512-cB58. In Figure 21 we show the spectrum of Arc 384 together with the spectrum of 1512-cB58, and the models with Salpeter and Miller-Scalo IMF described above. The similarities between the two lensed galaxies spectra are evident. Unfortunately, the signal-to-noise of Arc 384 is not as high as in 1512-cB58. However, the general features are again reproduced and we can confirm that this galaxy is a star-forming galaxy at  $z = 2.515$ .

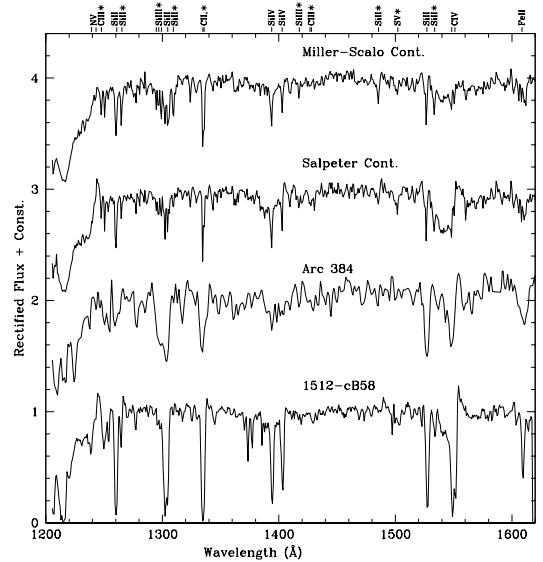


Fig. 21.— Spectra of 1512-cB58, Arc 384, and synthetic spectra for two models: Salpeter IMF, continuous star-formation, 100 Myr, solar metallicity; Miller-Scalo IMF, continuous star-formation, 100 Myr, solar metallicity. Excited lines (photospheric) are marked with “\*”. “,\*” is used when only the second component is an excited line. The spectra are rectified.

## 7. Summary and Conclusions

The addition of the B star library to our synthesis code allows detailed studies of the stellar population of star-forming galaxies. We summarize our conclusions as follows.

- (1) The contribution of B stars in the UV line spectrum becomes important for greater ages ( $t > 5$  Myr) when O stars have evolved. By analyzing the changes in the profiles of several UV lines such as C III  $\lambda 1247$ , Si II  $\lambda 1261$ , 1265, Si II  $\lambda 1304$ , 1309, C II  $\lambda 1335$ , 1336, Si IV  $\lambda 1400$ , Si II  $\lambda 1485$ , Si II  $\lambda 1527$ , 1533,

Table 5: 1512-cB58 Data

Band	$\lambda_{\text{obs}}$ (Å)	$\lambda_{\text{rest}}$ (Å)	AB	$\lambda F_{\lambda}$ (erg cm <sup>-2</sup> s <sup>-1</sup> )	$\lambda P_{\lambda}$ (erg s <sup>-1</sup> )	$A_{\lambda}$	$L_{\text{final}}$ $L_{\odot}$	$L_{\text{model}}$ $L_{\odot}$	SFR (M <sub>⊙</sub> yr <sup>-1</sup> )
V	5500	1480	20.64	$1.1 \times 10^{-13}$	$6.15 \times 10^{45}$	3.6	$10^{45.53}$	$10^{43.61}$	83
K	21400	5750	19.61	$7.30 \times 10^{-14}$	$4.08 \times 10^{45}$	1.6	$10^{44.55}$	$10^{42.91}$	44

$L_{\text{final}}$  = Luminosity corrected for extinction and divided by 50 (magnification factor)

$L_{\text{model}}$  = Luminosity from Starburst99

C IV  $\lambda 1550$ , and Al II  $\lambda 1671$  it is possible to date the burst of star formation and to recognize the main contributors to the spectrum.

(2) Silicon is found to be a good diagnostic for spectral classification of B stars and lines such as Si III  $\lambda 1295$ , 1297, 1299, Si II  $\lambda 1265$ , Si III  $\lambda 1417$ , and Si II  $\lambda 1485$  are found to be good age indicators.

(3) Excited photospheric lines such as C III  $\lambda 1247$ , Si II  $\lambda 1265$ , Si III  $\lambda 1295$ , 1297, 1299, Si III  $\lambda 1417$ , C III  $\lambda 1426$ , Si II  $\lambda 1485$ , S V  $\lambda 1502$ , and Si II  $\lambda 1533$  have no interstellar contamination and are found to be the best diagnostic of the stellar population. However, some are intrinsically weak and require high signal-to-noise and high spectral resolution in order to be detected.

(4) Lines with strong P Cygni profiles such as N V  $\lambda 1239$ , 1243, Si IV  $\lambda 1400$ , and C IV  $\lambda 1550$  are found mainly when the stellar population is dominated by O stars and B supergiants. The P Cygni profile of C IV  $\lambda 1550$  is detected at earlier ages than Si IV  $\lambda 1400$  because of the larger optical depth of C<sup>3+</sup> in the wind.

(5) We used the GHRS high signal-to-noise spectrum of the super star cluster NGC 1705-1 to test our models. We found that the UV line spectrum is dominated by the light from B stars. The model that best reproduces the spectrum of NGC 1705-1 has a Salpeter IMF and instantaneous star formation. Photospheric lines of C III  $\lambda 1247$ , Si III  $\lambda 1417$ , and S V  $\lambda 1502$  were used as diagnostics to date the burst of NGC 1705-1 at 10 Myr.

(6) Broadening and blueshifts of several resonance lines are found to be stronger in NGC 1705-1 than in our models and are confirmed to be intrinsic of the galaxy. Si II  $\lambda 1261$  and Al II  $\lambda 1671$  were found to be pure interstellar lines with an average blueshift of 78 km s<sup>-1</sup> due to a directed outflow of the interstellar medium.

(7) We used the Keck high signal-to-noise spectrum of the gravitationally lensed galaxy 1512-cB58 ( $z = 2.723$ ) as a first application of our models to high-redshift galaxies. Direct comparison between 1512-

cB58 and NGC 1705-1 showed that both spectra have many strong absorption features in common. However, the P Cygni profiles in 1512-cB58 suggest that this galaxy has O stars in addition.

(8) Models with continuous star formation were found to be more adequate for 1512-cB58 since there are spectral features typical of a composite stellar population of O and B stars. A model with  $Z = 0.4 Z_{\odot}$  and an IMF with  $\alpha=2.8$  reproduces the stellar features of 1512-cB58 spectrum.

We have demonstrated that our method is able to reproduce the spectral features of galaxies at low- and high- $z$ , although high signal-to-noise and high spectral resolution are needed in order to distinguish the stellar features typical of B stars. High spectral resolution is very important in this method since many of the photospheric lines are very close to interstellar lines and deblending becomes crucial. In the two cases analyzed, NGC 1705-1 and 1512-cB58, the contribution of massive stars to the spectra is easily identified via diagnostic lines. The full potential of this method can be exploited in the near future when high-quality spectra of local and distant star-forming galaxies will be obtained with the new generation of ground-based and space telescopes.

We are grateful to Richard Ellis for providing us with the spectrum of Arc 384, Ivan Hubeny and Derck Massa for helpful comments, Sandra Savaglio for valuable suggestions, R. Thompson for helping with IDL and echelle orders combination, Nolan Walborn for his comments on this manuscript, and Tommy Wiklund for providing the  $\chi^2$  routine. We acknowledge NASA support for this research from an ADP grant (No. NAG5-6903) and LTSA grant (No. NAGW-3138).

## REFERENCES

- Bieging, J. H., Abbott, D. C., & Churchwell, E. B. 1989, ApJ, 340, 518
- Blaha, C., & Humphreys, R. M. 1989, AJ, 98, 1598 (BH)

- Calzetti, D. 1997, *AJ*, 113, 162
- Castor, J. I., Abbott, D. C., & Klein, R. I. 1975, *ApJ*, 195, 157
- Chlebowski, T., & Garmany, C. D. 1991, *ApJ*, 368, 241
- Dey, A., van Breugel, W., Vacca, W. D., & Antonucci, R. 1997, *ApJ*, 490, 698
- Ebbels, T. M. D., Le Borgne, J.-F., Pelló, R., Ellis, R. S., Kneib, J.-P., Smail, I., & Sanahuja, B. 1996, *MNRAS*, 281, L75
- Ellingson, E., Yee, H. K. C., Bechtold, J., & Elston, R. 1996, *ApJ*, 466, L71
- Fanelli, M. N., O'Connell, R. W., & Thuan, T. X. 1988, *ApJ*, 334, 665
- Gioia, I. M., & Luppino, G.A. 1994, *ApJS*, 94, 583
- Groenewegen, M. A. T., & Lamers, H. J. G. L. M. 1989, *A&AS*, 79, 359
- Heckman, T. M. 1997, in *Star Formation Near and Far: Seventh Astrophysics Conference*, ed. S. S. Holt & L. G. Mundy. (Woodbury: AIP), 271
- Heckman, T. M., & Leitherer, C. 1997, *AJ*, 114, 69
- Heckman, T. M., Robert, C., Leitherer, C., & Garnett, D. R. 1998, *ApJ*, 503, 646
- Howarth, I. D., Siebert, K. W., Hussain, G. A. J., & Prinja, R. K. 1997, *MNRAS*, 284, 265
- Huchra, J. P., Geller, M. J., Gallagher, J., Hunter, D., Hartmann, L., Fabbiano, G., & Aaronson, M. 1983, *ApJ*, 274, 125
- Humphreys, R. M., & McElroy, D. B. 1984, *ApJ*, 284, 565
- Kinney, A. L., Bohlin, R. C., Calzetti, D., Panagia, N., & Wyse, R. F. G. 1993, *ApJS*, 86, 5
- Leitherer, C. 1999a, in *Chemical Evolution from Zero to High Redshift*, ed. J. Walsh & M. Rosa, (Berlin: Springer), in press
- Leitherer, C., Ferguson, H. C., Heckman, T. M., & Lowenthal, J. D. 1995a, *ApJ*, 454, L19
- Leitherer, C., Fritze-v. Alvensleben, U., & Huchra, J. 1996, *From Stars to Galaxies — The Impact of Stellar Physics on Galaxy Evolution* (San Francisco: ASP)
- Leitherer, C., & Heckman, T. M. 1995b, *ApJS*, 96, 9
- Leitherer, C., Robert, C., & Heckman, T. M. 1995c, *ApJS*, 99, 173
- Leitherer, C., Schaerer, D., Goldader, J., Gonzalez-Delgado, R. M., Robert, C., Kune, D. F., de Mello, D. F., Devost, D., & Heckman, T. 1999b, *ApJS*, 123, 3 (Starburst99)
- Lejeune, T., Cuisinier, F., & Buser, R. 1997, *A&AS*, 125, 229
- Lucy, L. B., & Solomon, P. M. 1970, *ApJ*, 159, 879
- Maeder, A., & Conti, P. S. 1994, *ARA&A*, 32, 227
- Marlowe, A. T., Heckman, T. M., Wyse, R. F. G., & Schommer, B. 1995, *ApJ*, 438, 563
- Massey, P., Lang, C. C., DeGioia-Eastwood, K., & Garmany, C. D. 1995, *ApJ*, 438, 188
- Melnick, J., Moles, M., & Terlevich, R. 1985, *A&A*, 149, 24
- Meurer, G., Freeman, K. C., Dopita, M. A., & Cacciari, C. 1992, *AJ*, 103, 60
- Meurer, G., Heckman, T. M., & Calzetti, D. 1999, in *After the Dark Ages: When Galaxies were Young (the Universe at  $2 < z < 5$ )*, ed. S. Holt, & E. Smith (Woodbury:AIP), 359
- Meurer, G., Heckman, T. M., Leitherer, C., Kinney, A., Robert, C., & Garnett, D. R. 1995, *AJ*, 110, 2665
- Miller, G. E., & Scalo, J. M. 1979, *ApJS*, 41, 513
- Moore, C. E. 1950, *An Ultraviolet Multiplet Table* (Washington: US Government Printing Office)
- Nemry, R., Surdej, J., & Hernaiz, A. 1991, *A&A* 247, 469
- Pettini, M. 1999, in *Chemical Evolution from Zero to High Redshift*, ed. J. Walsh & M. Rosa, (Berlin: Springer), in press
- Pettini, M., Steidel, C. C., Adelberger, K. L., Dickinson, M. E., & Giavalisco, M. 1999, *ApJ*, accepted
- Prinja, R. K. 1990, *MNRAS*, 246, 392
- Robert, C., Garnett, D. R., Heckman, T. M., Leitherer, C., Kinney, A. L., & Meurer, G., 1999, in preparation
- Robert, C., Leitherer, C., & Heckman, T. M. 1993, *ApJ*, 418, 749
- Rountree, J., & Sonneborn, G. 1993, *Spectral Classification With the International Explorer: An Atlas of B-Type Spectra* (NASA RP-1312)
- Sahu, M. S., & Blades, J. C. 1997, *ApJ*, 484, L125
- Salpeter, E. E. 1955, *ApJ*, 121, 161

- Schaller, G., Schaerer, D., Meynet, G., & Maeder, A. 1992, *A&AS*, 96, 269
- Schmidt-Kaler, T. 1982, in Landolt-Börnstein, New Series, Group VI, Vol. 2b, ed. K. Schaifers & H. H. Voigt (Berlin: Springer), 1
- Seitz, S., Saglia, R. P., Bender, R., Hopp, U., & Belloni, P. 1998, *MNRAS*, 298, 945
- Steidel, C. C., Giavalisco, M., Pettini, M., Dickinson, M., & Adelberger, K. 1996, *ApJ*, 462, L17
- Vacca, W. D., Robert, C., Leitherer, C., & Conti, P. S. 1995, *ApJ*, 444, 647
- Yee, H. K. C., Ellingson, E., Bechtold, J., Carlberg, R. G., & Cuillandre, J.-C., 1996, *AJ*, 111, 1783
- York, D. G., Caulet, A., Rybski, P., Gallagher, J., Blades, J. C., Morton, D. C., & Wamsteker, W. 1990, *ApJ*, 351, 412
- Walborn, N. R. 1971, *ApJS*, 23, 257
- Walborn, N. R., Lennon, D. J., Haser, S. M., Kudritzki, R.-P., & Voels, S. A. 1995a, *PASP*, 107, 104
- Walborn, N. R., Nichols-Bohlin, J., & Panek, R. J. 1985, *International Ultraviolet Explorer Atlas of O-Type Spectra from 1200 to 1900 Å* (NASA RP-1155)
- Walborn, N. R., Parker, J. W., & Nichols, J. S. 1995b, *International Ultraviolet Explorer Atlas of B-Type Spectra from 1200 to 1900 Å* (NASA RP-1363)